HHS Public Access

Author manuscript

Biomaterials. Author manuscript; available in PMC 2017 January 01.

Published in final edited form as:

Biomaterials. 2016 January ; 76: 66–75. doi:10.1016/j.biomaterials.2015.10.043.

MMP-mediated Mesenchymal Morphogenesis of Pluripotent Stem Cell Aggregates Stimulated by Gelatin Methacrylate Microparticle Incorporation

Anh H. Nguyen[1], **Yun Wang**[3], **Douglas E. White**[1], **Manu O. Platt**[1,2], and **Todd C. McDevitt**[3,4,*]

[1]The Wallace H. Coulter Department of Biomedical Engineering, Georgia Institute of Technology and Emory University, Atlanta, Georgia, USA

[2]The Parker H. Petit Institute of Bioengineering and Bioscience, Georgia Institute of Technology, Atlanta, Georgia, USA

[3]The Gladstone Institute for Cardiovascular Disease, San Francisco, California, USA

[4]Department of Bioengineering and Therapeutic Sciences, University of California San Francisco, San Francisco, California, USA

Abstract

Matrix metalloproteinases (MMPs) remodel the extracellular matrix (ECM) to facilitate epithelialto-mesenchymal transitions (EMTs) and promote cell specification during embryonic development. In this study, we hypothesized that introducing degradable ECM-based biomaterials to pluripotent stem cell (PSC) aggregates would modulate endogenous proteolytic activity and consequently enhance the differentiation and morphogenesis within 3D PSC aggregates. Gelatin methacrylate (GMA) microparticles (MPs) of low (~20%) or high (~90%) cross-linking densities were incorporated into mouse embryonic stem cell (ESC) aggregates, and the effects on MMP activity and cell differentiation were examined with or without MMP inhibition. ESC aggregates containing GMA MPs expressed significantly higher levels of total MMP and MMP-2 than aggregates without MPs. GMA MP incorporation increased expression of EMT markers and enhanced mesenchymal morphogenesis of PSC aggregates. MMP inhibition completely abrogated these effects, and GMA MP-induced MMP activation within ESC aggregates was partially reduced by pSMAD 1/5/8 inhibition. These results suggest that GMA particles activate MMPs by protease-substrate interactions to promote EMT and mesenchymal morphogenesis of ESC aggregates in an MMP-dependent manner. We speculate that controlling protease activity via the introduction of ECM-based materials may offer a novel route to engineer the ECM microenvironment to modulate stem cell differentiation.

* Address for Correspondence: Todd C. McDevitt, Ph.D., The Gladstone Institutes, 1650 Owens Street, San Francisco, CA 94158, Phone: 415-734-2875, **todd.mcdevitt@gladstone.ucsf.edu**.

Keywords

gelatin methacrylate; microparticles; matrix metalloproteinases; pluripotent stem cells; epithelial-to-mesenchymal transition; mesenchymal morphogenesis

1. Introduction

Pluripotent stem cells (PSCs) hold tremendous promise for regenerative medicine and tissue engineering. PSC aggregates enable complex cell-cell interactions and promote extracellular matrix (ECM) production in a manner that parallels embryogenesis and *in vivo* tissue development. Thus, 3D aggregates are valuable models for studying the multifaceted milieu required for PSC differentiation. Differentiation of PSC aggregates is strongly influenced by the biochemical composition of the culture medium, however, the 3D geometry of cell spheroids inherently limits the free diffusion and homogeneous presentation of soluble molecules throughout multicellular aggregates [2, 3]. We have previously demonstrated that biomolecule delivery from incorporated microparticles (MPs) results in more homogeneous delivery within aggregates than soluble treatments [2-4]. In fact, even incorporating “empty” biomaterial MPs within stem cell aggregates affects the relative differentiation trajectories based on cell-material interactions, even without the delivery of exogenous factors [3, 4]. In particular, extracellular matrix (ECM)-based materials have been increasingly used to direct stem cell differentiation, based on their innate ability to provide ECM cues for differentiation and maintenance of differentiated tissues [5-9] through remodeling by matrix metalloproteinases (MMPs) [10].

Direct ECM contact with cells has the potential to modulate MMP activity through a substrate-protease specific response. For example, cells cultured on 2-D surfaces coated with ECM molecules, such as decorin, vitronectin, and fibronectin, trigger enhanced amounts of active MMPs that specifically cleave these molecules [11-13]. Moreover, exposure of cells, particularly stem cells, to MMP-cleavable peptides enhances MMP levels and facilitates differentiation processes. For example, mesenchymal stem cells (MSCs) cultured in an RGD-alginate gel with MMP-cleavable peptides had greater MMP-2 activity than MSCs cultured only in an RGD-alginate gel [14]. Also, increasing the concentration of an MMP-cleavable peptide cross-linker in PEG hydrogels enhances MMP-2 activity of cultured MSCs in a proportional manner [15]. Furthermore, when human MSCs were cultured in type I collagen-rich 3D gels, elevated membrane-tethered MMP (MT1-MMP) activity was responsible for hMSC collagenolytic and invasive activity and osteogenic potential [16]. Thus, cell interactions with ECM materials can promote MMP activity, which may facilitate ECM remodeling and cell differentiation.

MMPs modulate many differentiation processes via cleavage of ECM molecules that in turn release sequestered growth factors and expose ECM motifs that stimulate receptor-mediated signaling cascades to promote downstream transcriptional activity [17]. In particular, remodeling of the ECM by matrix metalloproteinases (MMPs) is critical to the epithelial-to mesenchymal transition (EMT) that occurs after primitive streak formation and leads to formation of all 3 germ layers during gastrulation [18, 19]. Specifically, MMPs facilitate

epiblast cell ingression through the primitive streak to form mesoderm and definitive endoderm through MMP-mediated breakdown of the basement membrane [20, 21], which enables epithelial cell delamination and migration, and also release of matrix-bound molecules and exposure of “cryptic sites” in ECM that can induce transcriptional repression of epithelial markers, such as E-cadherin, and stimulation of mesenchymal markers, including N-cadherin, fibronectin, and MMP-2 and -9 [22-28].

Differentiation of PSC aggregates recapitulates many of the multicellular morphogenic programs of embryological development, but although the roles of MMPs have been extensively characterized within mammalian and avian embryogenesis [21, 22, 29, 30], relatively little is known about how MMP-mediated ECM remodeling can regulate differentiation of pluripotent stem cells [31]. Additionally, although cell-contact with substrate-specific materials can trigger enhanced MMP activity, the increased activity depends on 2-D vs. 3-D presentation [32]. We hypothesized that incorporation of enzymatically degradable MPs composed of gelatin within PSC aggregates would increase MMP activity, promote EMT-like processes, and ultimately enhance mesendodermal differentiation. The critical roles of MMPs and extracellular remodeling in early embryogenesis strongly suggest that introducing degradable ECM materials into stem cell 3D microenvironments could offer a novel route to direct PSC differentiation and morphogenesis.

2. Materials and Methods

2.1. Mouse ESC culture

Undifferentiated mouse embryonic stem cells (mESCs) (D3) (passages 23-33) were cultured on 0.1% gelatin-coated tissue-culture dishes in ESC medium composed of DMEM (Mediatech, Herndon, VA) supplemented with 15% FBS (Hyclone, Logan, UT), 1× non-essential amino acids (Mediatech), 2 mM L-glutamine (Mediatech), 100 U/ml penicillin, 100 μg/ml streptomycin, and 0.25 μg/ml amphotericin (Mediatech), 0.1 mM 2-mercaptoethanol (Fisher Scientific, Fair Lawn, NJ), and 10^3 U/ml leukemia inhibitory factor (LIF) (Millipore, Billerica, MA). mESCs were routinely passaged with 0.05% trypsin every 2–3 days before reaching 70% confluency.

2.2. Microparticle formulations

Gelatin methacrylate (GMA) MPs with 20% and 90% cross-linking densities (~5 μm diameter) were fabricated via a water-in-oil emulsion as previously described [33]. In some cases, GMA MPs were fluorescently labeled by incubation with Alexa-Fluor 594 succidimidyl ester (Invitrogen, Carlsbad, CA) in a 0.1 M sodium bicarbonate buffer, followed by four washes with deionized water before aggregate incorporation. Heparin methacrylate MPs were synthesized as described [34]. Poly (methyl) methacrylate (Polysciences, Warrington, PA) and polystyrene MPs (Spherotech, Lake Forest, IL) of similar sizes (5–10 μm) were purchased. GMA-coated polystyrene MPs were made by incubating polystyrene MPs with a 1% sterile filtered GMA solution for 2 hours at room temperature, followed by three washes in PBS with 1% BSA.

2.3. ESC spheroid formation and culture

mESCs were treated with 0.05% trypsin to obtain a single-cell suspension and aggregated within AggreWell™ 400 inserts (Stem Cell Technologies, Vancouver, Canada). Briefly, 1.2×10^6 cells in 0.5 mL of medium were inoculated into the microwell inserts and centrifuged at 200 g for 5 minutes to distribute the cells among the ~1200 individual microwells/insert. For MP incorporation, 1.2×10^6 cells were homogeneously mixed with 0.4, 1.2, or 3.6×10^6 MPs with seeding ratios of 1:3, 1:1, or 3:1 (MPs:cells) immediately before adding them to the microwell inserts. After 18 hours of culture, a wide-bore pipette was used to remove cell aggregates from the microwells and transfer them to a rotary orbital shaker (45 rpm) for suspension culture. Spheroids were collected by sedimentation every 2 days, and 90% of the medium was exchanged with fresh mESC medium (without LIF). The MMP inhibitor, Ro32-3555 (Tocris Biosciences, Bristol, UK), was initially added at 50 μM on day 5 and every other day thereafter with medium exchanges, and the pSMAD inhibitor, LDN-193189 (Stemgent, Cambridge, MA), was first added at 0.2 μM on day 3 and every other day thereafter with each media exchange.

2.4. MP incorporation analysis

MP-incorporated spheroids were collected from microwells after 18 hours, and the spheroids were counted with a hemocytometer and then lysed in a solution of 5% SDS and 0.1 NaOH for 2 hours at room temperature. The incorporated MPs in the lysate from a known number of spheroids were counted to calculate the MP incorporation that was expressed as numbers of incorporated MPs per spheroid. Fluorescently-labeled GMA MPs within the spheroid lysate were analyzed on a Synergy H4 plate reader (Biotek, Winooski, VT) (emission 570 nm, excitation 620 nm). The number of microparticles was determined using a standard curve obtained with a known number of microparticles suspended in the lysis solution. Non-florescent labeled GMA, heparin methacrylate, poly (methyl) methacrylate, and polystyrene MPs in the lysate were directly counted on a hemocytometer.

2.5. MMP activity analysis

Overall protease activity was measured with the Sensolyte® 520 Generic MMP Assay Kit (AnaSpec, San Jose, CA) as described [35, 36]. The kit uses a quenched FAM/QXL FRET-conjugated universal MMP sensitive peptide sequence. Spheroids were lysed by homogenization on ice in 0.1% Triton-X in the provided assay buffer, followed by centrifugation and collection of the supernatant lysate. Lysates were treated with 1 mM amino-phenyl mercuric acetate (APMA) for 2 hours to activate zymogen MMPs and assayed alongside non-APMA-treated counterparts to quantify total and active levels, respectively. Equal volumes of the spheroid lysate and FRET-conjugated substrate (50 μL) were incubated in a black 96-well plate for 1 hour at room temperature before adding stop solution and reading the plate on a Synergy H4 plate reader at excitation/emission: 490 nm/520 nm. A standard curve was created using a 5-FAM fluorescence reference to convert fluorescence values into the amount of cleaved substrate and calculated values were normalized to total protein content (determined by a BCA assay) and compared to samples that lacked MPs.

MMP-2 protease activity was analyzed by zymography. Undifferentiated mESCs (day 0) and aggregates with and without MPs from days 1, 4, 7, 10, and 14 of differentiation were homogenized on ice for 5 seconds with lysis buffer (20 mM Tris-HCl pH 7.5, 5 mM EGTA, 150 mM NaCl, 20 mM glycerol-phosphate, 10 mM NaF, 1 mM sodium orthovanadate, 1% Triton X-100, 0.1% Tween 20). The protein concentration in the supernatant was quantified, and 15 μg of protein was mixed with 5X non-reducing loading buffer (0.05% bromophenol blue, 10% SDS, 1.5 M Tris, 50% glycerol) before loading onto a 10% SDS-polyacrylamide gel containing 5 mg/mL gelatin. The gel was run at 4°C at 115 V, and then the gels were removed and the enzymes were renatured in 2.5% Triton X for 30 minutes and incubated overnight in an assay buffer containing 50 mM Tris-HCl, 10 mM $CaCl_2$, 50 mM NaCl, and 0.05% Triton X-100. Gels were then rinsed with deionized water and stained with Coomassie Blue for 1 hour at room temperature. The gels were imaged using Imagequant 4010 (GE Healthcare, Amersham, UK). Band intensities were analyzed by densitometry using ImageJ software (NIH, Bethesda, MD).

2.6. Gene expression analysis

Total RNA was extracted from undifferentiated ESC monolayers and spheroid samples at days 7, 10, and 14 of differentiation with the RNeasy Mini kit (Qiagen, Valencia, CA). Complementary cDNA was obtained via the iScript cDNA synthesis kit (Bio-Rad, Hercules, CA) and analyzed using SYBR green technology and real-time PCR (MyIQ cycler, Bio-Rad). Sequences and annealing temperatures for Mixl1, Brachyury-T, E-Cadherin, N-Cadherin, Snai1, Slug, Mesp1, MMP-2, Flk1, Pax6, FoxA2, Nanog, and *18S* are provided in supplementary Table 1. Gene expression levels were normalized to the housekeeping gene 18S and calculated with respect to expression levels of undifferentiated mESCs by the Pfaffl method [37].

2.7. Histology and immunostaining

Spheroids were fixed in 10% formalin, entrapped in Histogel (Thermo Scientific, Rockford, IL), and processed and embedded in paraffin. Paraffin blocks were sectioned to 5 μm thickness (Microm HM 355S) and adhered to Superfrost Plus slides (VWR, West Chester, PA). The sections were deparaffinized, stained with hematoxylin and eosin (H&E), and imaged with a Nikon 80i upright microscope equipped with a SPOT Flex camera (15.2 64 MP Shifting Pixel, Diagnostic Instruments, Sterling Heights, MI).

For whole-mount immunofluorescent staining, spheroids were permeabilized for 30 minutes in 1.5% Triton X-100 in blocking buffer of 2% serum of the same animal origin as the Alexa-Fluor-conjugated secondary antibodies (Invitrogen, Carlsbad, CA, goat or donkey, 1:200) against N-cadherin (Dako, Glostrup, Denmark, mouse monoclonal, 1:30), E-cadherin (Sigma, St. Louis, MO, rat polyclonal, 1:200), fibronectin (Millipore, Temecula, CA, rabbit polyclonal, 1:80), and α-smooth muscle actin (Dako, mouse monoclonal, 1:100). The spheroids were incubated with primary antibody in blocking buffer overnight at 4°C, rinsed with 0.1% Tween in PBS, and incubated with secondary antibody in blocking buffer for 4 hours at 4°C. Spheroids were counterstained with Hoechst (1:100), washed 3 times in 0.1% Tween with PBS and imaged using a Zeiss LSM 700 confocal microscope (Carl Zeiss, Heidelberg, Germany).

2.8. Principal component analysis of mesenchymal morphogenesis

To extract quantitative network metrics from images, digital networks were created using Cell Profiler. Briefly, H&E histological images were loaded into Cell Profiler [38], and the cytoplasm-versus-nuclear staining was separated using the spectral separation algorithm. Individual cells were identified via nuclei, and cell bodies were extended to match cytoplasmic boundaries using CellProfiler's “expand” function. Various metrics related to shape (e.g., area, perimeter, eccentricity) were measured using the “measure object size shape” module. Neighboring cells for each cell were counted with “get nearest neighbors” module. Data were exported and processed using custom Python files to create multicellular networks while retaining individual cell shape information.

A machine-learning algorithm was applied to the resulting networks to extract features that could provide classification information about the cell type. The resulting classifiers were trained using information on cell physical shape and morphology and metrics derived from the network analysis, such as the number of neighbors and connection length. Various classifiers from the sklearn package were tested, although ultimately a SVM-based approach was used.

Principal component analysis (PCA) was performed using the sklearn Python package based on the algorithm outlined in Tipping et al. [39] that uses a probabilistic approach coupled with singular value decomposition. Data management and loading heatmaps were generated using custom python code and scores plots were generated using the scatter function from Matplotlib in Python.

2.9. Statistical analysis

All values are reported as mean ± standard error, for at least triplicate independent biological samples. Before performing statistical analysis, all non-normal data were Box-Cox transformed to obtain a Gaussian distribution by MATLAB software (Natick, MA). Statistical significance was determined via one-way ANOVA with Tukey's post hoc analysis with 95% confidence intervals after performing Levene's equality of variances test on SYSTAT 12 software (Chicago, IL). P-values < 0.05 were considered to be statistically significant.

3. Results

3.1. MP incorporation increases matrix metalloproteinase levels

The 20% and 90% GMA MP formulations (Figure 1A) were initially seeded at MP:cell ratios of 1:3, 1:1, and 3:1 and resulted in about 200, 600, and 1200 MPs per spheroid, corresponding to an incorporation ratio of 1:5, 3:5, and 1.2:1 (MPs:cells), respectively (Figure 1B, Supplemental Figure 1). However, after transferring to suspension culture, spheroids with a seeding density higher than 1:3 MPs:cells quickly agglomerated to form large masses. Thus, the 1:3 MPs:cells seeding ratio was used for the remainder of the studies. Both of the MP formulations seeded at a 1:3 MPs:cells ratio persisted within the spheroid for up to 14 days of rotary culture, as illustrated by the continued presence of Alexa-Fluor-labeled MPs (red) in the aggregates (Figure 1C).

Overall MMP expression in spheroids was assessed in response to MP incorporation (Figure 2A). Total MMP levels peaked at day 10, while active MMP levels appeared to remain constant throughout the course of differentiation. On day 4, spheroids with 20% GMA MPs had more total and active MMP than the no-MP spheroids. On day 7, spheroids with both MP formulations exhibited greater total and active MMP levels than the no-MP spheroids. The highest MMP levels were observed in spheroids containing 90% GMA MPs.

Similar to the changes in overall MMP activities, the level of MMP-2 also peaked at day 10 and was higher in the presence of GMA MPs, as demonstrated by zymography and densitometry analyses (Figure 2B, C). The pro form of MMP-2 was detected throughout the entire time course analyzed, and the active form was observed on days 7–14. Incorporation of the 20% GMA MPs (20%) led to a significant increase of MMP-2 pro form as early as day 1. By day 7, spheroids with both MP formulations had more pro form than spheroids lacking MPs, and this lasted until day 14. The highest increase (i.e., 3.1-fold more than no-MP spheroids) was observed in 20% GMA aggregates at day 10. Furthermore, those with 90% GMA particles had more of the MMP 2 active form than the no-MP or 20% GMA aggregates at days 7 and 10.

The effects of GMA alone on MMP activity were also examined by plating day 4 spheroids on either tissue culture polystyrene (TCPS) plates or TCPS plates coated with 20% or 90% cross-linked GMA. In all cases, spheroids expressed comparable amounts of MMP-2 pro and active forms of MMP-2 at day 7, regardless of GMA coating (Figure 2D). Furthermore, to determine the specificity of the MMP-2 response to GMA materials, MPs of similar size but different chemical compositions to that of GMA MPs (e.g., polystyrene (PS), PS coated with either 20% or 90% GMA, poly (methyl) methacrylate (PMMA), and heparin methacrylate (Hep) MPs) were incorporated at comparable amounts into spheroids when seeded at 1:3 MPs:cells. However, none of the other materials, besides GMA MPs, enhanced MMP-2 levels at day 1 or 7 of differentiation (Supplemental Figure 2). These results indicated that both 3D presentation and GMA chemistry are essential to increase MMP production and activation in ESC aggregates.

3.2. GMA MPs regulate EMT-related gene and protein expression patterns

We next determined if the enhanced MMP activity by GMA MP incorporation affected the expression patterns of EMT-related molecules at day 10 of differentiation based upon the ability of proteases to facilitate EMT processes. Spheroids without MPs primarily expressed E-cadherin at the extracellular membrane, whereas those with MPs exhibited a punctate pattern, suggesting degradation of E-cadherin (Figure 3A). More N-cadherin was expressed within the interior of spheroids with GMA MPs than those without (Figure 3B). Moreover, fibronectin expression was observed throughout the spheroids (Figure 3C) and frequently co-localized with MMP-2 (Figure 3D). Particularly large fibrillar regions of fibronectin were seen in 90% GMA MP spheroids (Figure 3C). Noticeably, strong expression of MMP-2 was detected in punctate regions about the same size and shape of MPs only within spheroids containing GMA MPs (Figure 3D, Supplemental Figure 3).

Incorporation of GMA MPs also changed the gene expression pattern of various phenotypic markers. Compared to aggregates without MPs, reduced expression of the primitive streak

genes, *mixl1* and *brachyury-T* was observed in MP aggregates on day 4 (Figure 4A), but the expression of EMT and early mesendodermal differentiation markers, including *N-cadherin, mesp1*, and *gata4,* was significantly higher in MP spheroids, particular with 90% GMA MPs on day 7. While *E-cadherin* expression was not differentially affected, the level of *Slug*, an E-cadherin repressor, was increased in 20% GMA MP spheroids on day 7. In agreement with the changes of MMP-2 at the protein level, MP incorporation also led to an increase in *mmp-2* mRNA on day 7 (Figure 4B). As expected, *nanog* (pluripotent marker) expression levels decreased similarly across all spheroid groups as differentiation progressed (Figure 4C). However, mesendodermal differentiation appeared to be specifically affected by GMA MP incorporation: expression of *foxA2* (endoderm) and *flk1* (mesoderm) was increased at day 7 and/or day 10, but there were no differences in *pax6* (ectoderm) at any time examined.

3.3. MMP inhibition abrogates MP-induced EMT-related gene expression

Based on the appearance of active MMP-2 by day 7, an MMP inhibitor (Ro32-3555) was supplemented to the spheroid cultures starting at day 5 and a concomitant decrease in active MMP-2 in all spheroid groups was observed up to 14 days of differentiation (Supplemental Figure 4). MMP inhibition resulted in a three-fold increase in expression of *Mixl1* in the 90% GMA MP spheroids, while *brachyury-T* expression was unaffected (Figure 5A). Furthermore, GMA MP-induced increases in gene expression of EMT markers (*N-cadherin* and *Slug*), *mmp-2*, and early and later mesendodermal markers (*mesp1, gata4, foxa2*, and *flk1*) were completely abrogated by MMP inhibitor treatment, and their expression levels were comparable to those in non-MP vehicle control groups (Figure 5B, C). Although *nanog* expression was not affected, *pax6* expression in 90% GMA MP spheroids was reduced by MMP inhibition (Figure 5C).

3.4. Mesenchymal morphogenesis stimulated by MP incorporation is MMP-dependent

In parallel with differentiation marker expression, we also examined the morphological organization of ESC multicellular aggregates in response to MP incorporation throughout differentiation. By day 7, all spheroids initially exhibited similar homogeneous populations of cells with densely packed, epithelial-like morphologies. Starting at day 10 of differentiation, histological differences were observed between spheroids with or without GMA MPs. GMA MP-containing spheroids began to exhibit more cavitation, representative of internal spheroid remodeling, but the spheroids without MPs retained a tightly packed epithelial-like phenotype (Supplemental Figure 5). By day 14, spheroids with MPs, particularly the 90% GMA MPs, were composed of many spindle-shaped, mesenchymal-like cells that occupied large regions of lower cell densities, and stained positively for α-smooth muscle actin (αSMA), a mesenchymal marker (Figure 6A, Supplemental Figure 5).

MMP inhibition resulted in a reduction in the appearance of cavitated structures and mesenchymal-like regions with αSMA+ staining by day 14 (Figure 6A, Supplemental Figure 5). The variance in mesenchymal phenotype was described by a PCA model based on cell morphology and cell cluster size and shape, which were separated along the first and second principal components, respectively (Figure 6B). PCA 1 and 2 accounted for 72.2% of the original variance in all samples. Incorporation of GMA MPs resulted in increased mesenchymal-like cell differentiation, and the 20% GMA MPs had the largest areas and

frequencies of mesenchymal-like cell clusters. MMP inhibition yielded an enhanced epithelial-looking cell population in the MP spheroids, with the largest areas and frequency of epithelial-like cell clusters in the 20% GMA MPs spheroids. In the absence of GMA MPs, MMP inhibition did not have a strong effect on the morphology of ESC spheroids (Figure 6).

3.5. pSMAD 1/5/8 inhibition reduced MP-induced MMP-2 activity in MP incorporated spheroids

GMA MPs can bind to BMPs [33] that can activate the SMAD 1/5/8 pathway to induce EMT and mesodermal differentiation of ESCs [40, 41]. To explore the possible involvement of SMAD signaling by which MPs regulate cell differentiation and MMP levels in ESC aggregates, we examined the mesenchymal morphology and MMP-2 levels in GMA MP spheroids after inhibiting SMAD 1/5/8 phosphorylation. SMAD 1/5/8 inhibitor (LDH-193189) prevented the appearance of mesenchymal cell phenotypes (Fig. 7A) and completely reduced the active form of MMP-2 in all of the spheroid groups at days 7 and 10 of differentiation (Fig. 7B).

4. Discussion

This study demonstrated that mesenchymal differentiation is enhanced in an MMP-dependent manner by incorporating degradable GMA MPs within 3D ESC aggregates. The enhancement of MMP-2 activity stimulated by GMA MPs was specific to the chemical composition and 3D presentation of MPs within ESC aggregates. GMA MP-induced EMT gene expression patterns and mesenchymal morphogenesis was abrogated by MMP inhibition, indicating the dependence on MMP activity for these processes to occur. pSMAD 1/5/8 inhibition also reduced MP-induced MMP-2 activity, suggesting that SMAD signaling mediates MMP-2 activity within ESC spheroids in response to GMA MP incorporation.

GMA MP incorporation enhanced MMP production at the mRNA and protein levels as well as protease activity. Thus, we sought to understand the conditions that elicit this proteolytic response. We found the effect of MP incorporation on MMP expression and activation in ESC aggregate depended on the MP chemical composition since no materials investigated in this study, other than GMA-based MPs, enhanced MMP-2 activity. Unlike studies in which leukocytes exposed to PMMA exhibited enhanced MMP-2 activity [42, 43], we found that the methacrylate chemistry in GMA did not enhance MMP activity since PMMA MPs did not increase MMP-2 levels within ESC aggregates. GMA-coated PS MPs did not increase MMP activity, likely due to the relatively little amount of GMA protein absorbed on PS MPs, especially compared to similar sized GMA MPs; this suggests that MPs with a minimum content of GMA may be required to induce MMP expression and activation within ESCs aggregates. Moreover, the manner of material presentation may also play a crucial role in inducing a proteolytic response, which may explain why MMP-2 production and activation did not increase when spheroids were plated on the GMA-coated 2D surface as opposite to the MMP responses in GMA incorporated MPs. Additionally, the greater MMP activity observed in spheroids in response to 90% rather than 20% GMA MPs might be attributed to the lower degradability of 90% GMA MPs as a result of the increased

crosslinking density of GMA [33] that might require more MMP activity to degrade the MPs – either greater amounts of MMP or longer periods of activation.

Increased MMP activity occurs during embryonic EMT to degrade basement membranes and facilitate epiblast cell ingression through primitive streak [21]. Coincident with increases in MMP, incorporation of GMA MPs resulted in a decline of primitive streak markers, followed by increased expression of EMT markers and mesendodermal markers in combination with the appearance of mesenchymal morphological changes during later stages of differentiation. MMP inhibition completely abrogated MP-induced activation of MMP during the period of primitive streak formation and largely inhibited the appearance of mesenchymal phenotypes within ESC aggregates. These results demonstrated that MP-induced MMP activation modulated the kinetics of differentiation in GMA MP aggregates. Future studies to further interrogate the mechanism of action of the GMA MPs on ESC differentiation could include addition of specific MMP isoforms to the culture media or engineering of the cells to silence or overexpress different MMPs. Additionally, MMPs mediate ECM remodeling and release of ECM-bound growth factors that are essential for embryogenesis and tissue morphogenesis, thus material-based induction of proteolytic activity may offer an innovative method to selectively modulate stem cell microenvironments and differentiation to generate desired cell types and tissue structures.

Alteration of cellular matrix recognition and adhesion that is required to increase cellular motility and invasion during EMT is partially achieved through changes in the expression of cadherin molecules [44]. MMP-mediated degradation of E-cadherin may be important in MP-induced EMT and mesenchymal differentiation. In particular, in mouse and human ESCs, MMP-2 cleaves laminin-111, a major component of the basement membrane to regulate the expression of E-cadherin and EMT-related processes [27]. Similarly, GMA MP incorporation led to the punctate expression of E-cadherin, suggesting E-cadherin internalization from the plasma membrane and degradation [45]. Furthermore, the increase of the E-cadherin repressor, *slug,* might facilitate E-cadherin internalization [41, 46]. Accompanied by the loss of E-cadherin, the gain of N-cadherin is associated with EMT processes in differentiated ESCs [47]. Similarly, incorporation of GMA MPs led to a significant increase in *N-cadherin* gene expression with more abundant distribution of N-cadherin protein throughout aggregates. Concomitant with the switch from E-cadherin to N-cadherin expression, assembly of a fibronectin matrix is another well-documented hallmark of EMT [31, 48] that is essential for mesoderm development in mouse embryo [49]. The accumulation of a fibrillar fibronectin matrix that co-localized with MMP-2 was more pronounced within ESC aggregates containing GMA MPs than those without and could contribute to the enhancement of mesendoderm differentiation. MMP-2 activity can expose cryptic binding sites in fibronectin to assist the self-assembly into a fibrillar matrix that promotes EMT and mesoderm development [25, 26]. The high affinity for fibronectin [50] and MMP-2 for gelatin might explain the observed co-localization of MMP-2 and fibronectin within aggregates containing GMA MPs.

SMAD signaling stimulated by transforming growth factor beta (TGF-β) super family members promotes EMT and mesodermal commitment [23]. Similar to previous studies demonstrating the ability of gelatin MPs to bind growth factors including TGFβs and bone

morphogenic proteins (BMPs) [51, 52], BMPs have a strong affinity to GMA MPs [33]. Thus, GMA MPs could locally sequester growth factors within ESC aggregates and enhance MMP activation and subsequent mesenchymal commitment. In this study, inhibition of pSMAD 1/5/8 significantly reduced the appearance of mesenchymal cells as well as the increase of MMP-2 activity induced by GAM MPs, which might indicate that activation of SMAD signaling by GMA MPs might also contribute to the promotion of mesenchymal differentiation and activation of MMP.

5. Conclusion

This study demonstrates that morphogenic processes and cell differentiation can be promoted by incorporating degradable ECM-based MPs within ESC aggregates. Specifically, GMA MPs promoted EMT and mesenchymal commitment of ESC aggregates by increasing MMP expression and activity. Overall, these results suggest that controlling protease activity via the introduction of ECM-based materials may offer a novel route to engineer the stem cell microenvironment to modulate differentiation.

Supplementary Material

Refer to Web version on PubMed Central for supplementary material.

Acknowledgments

Financial support was provided by funding from the National Institutes of Health (GM088291). AHN was supported by an NIH training grant (GM008433) and DEW was supported by an NSF IGERT (NSF DGE 0965945). The authors would like to thank Dr. Philip Keegan, Dr. Ivana Parker, Catera Wilder, and Christian Rivera for their advice with ESC zymography protocol development, as well as Miguel Monteiro for performing zymography assays.

References

1. Ten Berge D, Koole W, Fuerer C, Fish M, Eroglu E, Nusse R. Wnt signaling mediates self-organization and axis formation in embryoid bodies. Cell Stem Cell. 2008; 3:508–18. [PubMed: 18983966]
2. Carpenedo RL, Bratt-Leal AM, Marklein RA, Seaman SA, Bowen NJ, McDonald JF, et al. Homogeneous and organized differentiation within embryoid bodies induced by microsphere-mediated delivery of small molecules. Biomaterials. 2009; 30:2507–15. [PubMed: 19162317]
3. Bratt-Leal AM, Carpenedo RL, McDevitt TC. Engineering the embryoid body microenvironment to direct embryonic stem cell differentiation. Biotechnol Progr. 2009; 25:43–51.
4. Bratt-Leal AM, Carpenedo RL, Ungrin MD, Zandstra PW, McDevitt TC. Incorporation of biomaterials in multicellular aggregates modulates pluripotent stem cell differentiation. Biomaterials. 2011; 32:48–56. [PubMed: 20864164]
5. Kleinman HK, Philp D, Hoffman MP. Role of the extracellular matrix in morphogenesis. Curr Opin Biotech. 2003; 14:526–32. [PubMed: 14580584]
6. Daley WP, Peters SB, Larsen M. Extracellular matrix dynamics in development and regenerative medicine. J Cell Sci. 2008; 121:255–64. [PubMed: 18216330]
7. Chen SS, Fitzgerald W, Zimmerberg J, Kleinman HK, Margolis L. Cell-cell and cell-extracellular matrix interactions regulate embryonic stem cell differentiation. Stem Cells. 2007; 25:553–61. [PubMed: 17332514]
8. Rozario T, DeSimone DW. The extracellular matrix in development and morphogenesis: A dynamic view. Dev Biol. 2010; 341:126–40. [PubMed: 19854168]

9. Cawston TE, Wilson AJ. Understanding the role of tissue degrading enzymes and their inhibitors in development and disease. Best Pract Res Cl Rh. 2006; 20:983–1002.
10. Visse R, Nagase H. Matrix metalloproteinases and tissue inhibitors of metalloproteinases - Structure, function, and biochemistry. Circ Res. 2003; 92:827–39. [PubMed: 12730128]
11. Huttenlocher A, Werb Z, Tremble P, Huhtala P, Rosenberg L, Damsky CH. Decorin regulates collagenase gene expression in fibroblasts adhering to vitronectin. Matrix Biol. 1996; 15:239–50. [PubMed: 8892224]
12. Huhtala P, Humphries MJ, Mccarthy JB, Tremble PM, Werb Z, Damsky CH. Cooperative signaling by alpha-5-beta-1 and alpha-4-beta-1 integrins regulates metalloproteinase gene-expression in fibroblasts adhering to bibronectin. J Cell Biol. 1995; 129:867–79. [PubMed: 7537277]
13. Damsky CH, Moursi A, Zhou Y, Fisher SJ, Globus RK. The solid state environment orchestrates embryonic development and tissue remodeling. Kidney Int. 1997; 51:1427–33. [PubMed: 9150454]
14. Fonseca KB, Maia FR, Cruz FA, Andrade D, Juliano MA, Granja PL, et al. Enzymatic, physicochemical and biological properties of MMP-sensitive alginate hydrogels. Soft Matter. 2013; 9:3283–92.
15. Leight JL, Alge DL, Maier AJ, Anseth KS. Direct measurement of matrix metalloproteinase activity in 3D cellular microenvironments using a fluorogenic peptide substrate. Biomaterials. 2013; 34:7344–52. [PubMed: 23830581]
16. Lu CL, Li XY, Hu YX, Rowe RG, Weiss SJ. MT1-MMP controls human mesenchymal stem cell trafficking and differentiation. Blood. 2010; 115:221–9. [PubMed: 19901267]
17. Mott JD, Werb Z. Regulation of matrix biology by matrix metalloproteinases. Curr Opin Cell Biol. 2004; 16:558–64. [PubMed: 15363807]
18. Vu TH, Werb Z. Matrix metalloproteinases: effectors of development and normal physiology. Gene Dev. 2000; 14:2123–33. [PubMed: 10970876]
19. Werb Z, Chin JR. Extracellular matrix remodeling during morphogenesis. Ann Ny Acad Sci. 1998; 857:110–8. [PubMed: 9917836]
20. Thiery JP, Acloque H, Huang RYJ, Nieto MA. Epithelial-mesenchymal transitions in development and disease. Cell. 2009; 139:871–90. [PubMed: 19945376]
21. Acloque H, Adams MS, Fishwick K, Bronner-Fraser M, Nieto MA. Epithelial-mesenchymal transitions: the importance of changing cell state in development and disease. J Clin Invest. 2009; 119:1438–49. [PubMed: 19487820]
22. Moustakas A, Heldin CH. Signaling networks guiding epithelial-mesenchymal transitions during embryogenesis and cancer progression. Cancer Sci. 2007; 98:1512–20. [PubMed: 17645776]
23. Xu J, Lamouille S, Derynck R. TGF-beta-induced epithelial to mesenchymal transition. Cell Res. 2009; 19:156–72. [PubMed: 19153598]
24. Egeblad M, Werb Z. New functions for the matrix metalloproteinases in cancer progression. Nat Rev Cancer. 2002; 2:161–74. [PubMed: 11990853]
25. Basbaum CB, Werb Z. Focalized proteolysis: Spatial and temporal regulation of extracellular matrix degradation at the cell surface. Curr Opin Cell Biol. 1996; 8:731–8. [PubMed: 8939664]
26. Sternlicht MD, Werb Z. How matrix metalloproteinases regulate cell behavior. Annu Rev Cell Dev Bi. 2001; 17:463–516.
27. Horejs CM, Serio A, Purvis A, Gormley AJ, Bertazzo S, Poliniewicz A, et al. Biologically-active laminin-111 fragment that modulates the epithelial-to-mesenchymal transition in embryonic stem cells. P Natl Acad Sci USA. 2014; 111:5908–13.
28. Reing JE, Zhang L, Myers-Irvin J, Cordero KE, Freytes DO, Heber-Katz E, et al. Degradation products of extracellular matrix affect cell migration and proliferation. Tissue Eng Pt A. 2009; 15:605–14.
29. Duong TD, Erickson CA. MMP-2 plays an essential role in producing epithelialmesenchymal transformations in the avian embryo. Dev Dynam. 2004; 229:42–53.
30. Murry CE, Keller G. Differentiation of embryonic stem cells to clinically relevant populations: Lessons from embryonic development. Cell. 2008; 132:661–80. [PubMed: 18295582]

31. Kim YS, Yi BR, Kim NH, Choi KC. Role of the epithelial-mesenchymal transition and its effects on embryonic stem cells. Exp Mol Med. 2014:46.
32. Haas TL, Davis SJ, Madri JA. Three-dimensional type I collagen lattices induce coordinate expression of matrix metalloproteinases MT1-MMP and MMP-2 in microvascular endothelial cells. J Biol Chem. 1998; 273:3604–10. [PubMed: 9452488]
33. Nguyen AH, McKinney J, Miller T, Bongiorno T, McDevitt TC. Gelatin methacrylate microspheres for controlled growth factor release. Acta Biomater. 2015; 13:101–10. [PubMed: 25463489]
34. Hettiaratchi MH, Miller T, Temenoff JS, Guldberg RE, McDevitt TC. Heparin microparticle effects on presentation and bioactivity of bone morphogenetic protein-2. Biomaterials. 2014; 35:7228–38. [PubMed: 24881028]
35. Hammoud L, Burger DE, Lu XR, Feng QP. Tissue inhibitor of metalloproteinase-3 inhibits neonatal mouse cardiomyocyte proliferation via EGFR/JNK/SP-1 signaling. Am J Physiol-Cell Ph. 2009; 296:C735–45.
36. Gueders MM, Bertholet P, Perin F, Rocks N, Maree R, Botta V, et al. A novel formulation of inhaled doxycycline reduces allergen-induced inflammation, hyperresponsiveness and remodeling by matrix metalloproteinases and cytokines modulation in a mouse model of asthma. Biochem Pharmacol. 2008; 75:514–26. [PubMed: 17950252]
37. Pfaffl MW. A new mathematical model for relative quantification in real-time RT-PCR. Nucleic Acids Res. 2001; 29:2002–7.
38. Carpenter AE, Jones TR, Lamprecht MR, Clarke C, Kang IH, Friman O, et al. CellProfiler: image analysis software for identifying and quantifying cell phenotypes. Genome Biol. 2006; 7:R100.1–11. [PubMed: 17076895]
39. Tipping ME, Bishop CM. Probabilistic principal component analysis. J Roy Stat Soc B. 1999; 61:611–22.
40. Kinney MA, Saeed R, McDevitt TC. Mesenchymal morphogenesis of embryonic stem cells dynamically modulates the biophysical microtissue niche. Sci Rep. 2014; 4 doi:10.1038/srep04290.
41. Richter A, Valdimarsdottir L, Hrafnkelsdottir HE, Runarsson JF, Omarsdottir AR, Ward-van Oostwaard D, et al. BMP4 promotes EMT and mesodermal commitment in human embryonic stem cells via SLUG and MSX2. Stem Cells. 2014; 32:636–48. [PubMed: 24549638]
42. Nakashima Y, Sun DH, Maloney WJ, Goodman SB, Schurman DJ, Smith RL. Induction of matrix metalloproteinase expression in human macrophages by orthopaedic particulate debris in vitro. J Bone Joint Surg Br. 1998; 80B:694–700. [PubMed: 9699840]
43. Reno F, Traina V, Cannas M. Adsorption of matrix metalloproteinases onto biomedical polymers: a new aspect in biological acceptance. J Biomat Sci-Polym E. 2008; 19:19–29.
44. Wheelock MJ, Shintani Y, Maeda M, Fukumoto Y, Johnson KR. Cadherin switching. J Cell Sci. 2008; 121:727–35. [PubMed: 18322269]
45. Le TL, Yap AS, Stow JL. Recycling of E-cadherin: A potential mechanism for regulating cadherin dynamics. J Cell Biol. 1999; 146:219–32. [PubMed: 10402472]
46. Mohamet L, Hawkins K, Ward CM. Loss of function of e-cadherin in embryonic stem cells and the relevance to models of tumorigenesis. Journal of oncology. 2011; 2011 doi:10.1155/2011/352616.
47. Spencer HL, Eastham AM, Merry CL, Southgate TD, Perez-Campo F, Soncin F, et al. E-cadherin inhibits cell surface localization of the pro-migratory 5T4 oncofetal antigen in mouse embryonic stem cells. Molecular biology of the cell. 2007; 18:2838–51. [PubMed: 17507657]
48. Kalluri R, Weinberg RA. The basics of epithelial-mesenchymal transition. J Clin Invest. 2009; 119:1420–8. [PubMed: 19487818]
49. George EL, Georges-Labouesse EN, Patel-King RS, Rayburn H, Hynes RO. Defects in mesoderm, neural tube and vascular development in mouse embryos lacking fibronectin. Development. 1993; 119:1079–91. [PubMed: 8306876]
50. Hunt GC, Singh P, Schwarzbauer JE. Endogenous production of fibronectin is required for self-renewal of cultured mouse embryonic stem cells. Exp Cell Res. 2012; 318:1820–31. [PubMed: 22710062]

51. Link DP, van den Dolder J, van den Beucken JJ, Wolke JG, Mikos AG, Jansen JA. Bone response and mechanical strength of rabbit femoral defects filled with injectable CaP cements containing TGF-beta 1 loaded gelatin microparticles. Biomaterials. 2008; 29:675–82. [PubMed: 17996293]

52. Bratt-Leal AM, Nguyen AH, Hammersmith KA, Singh A, McDevitt TC. A microparticle approach to morphogen delivery within pluripotent stem cell aggregates. Biomaterials. 2013; 34:7227–35. [PubMed: 23827184]

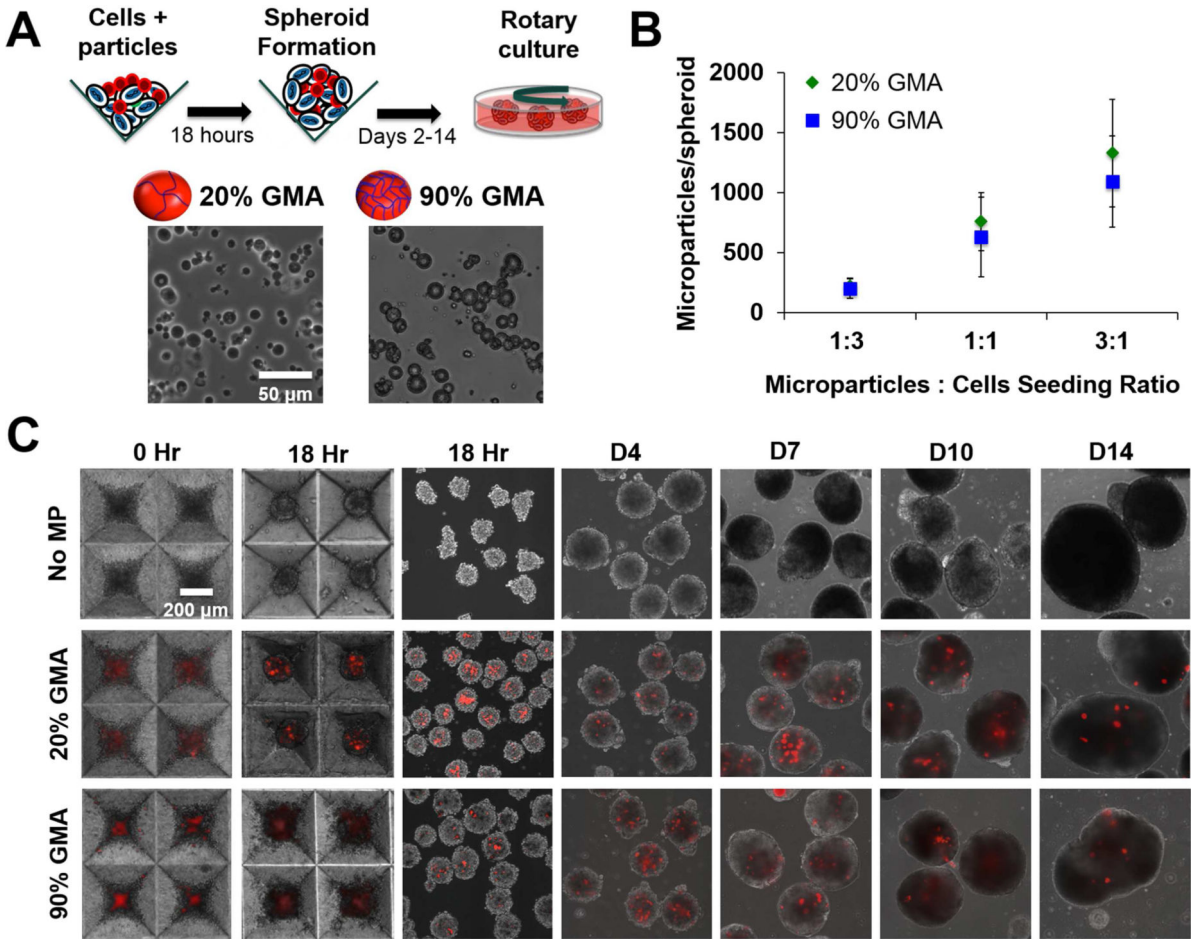

Figure 1.

GMA MP incorporation and persistence in ESC aggregates. (A) 20% and 90% GMA MPs were incorporated in ESC aggregates via forced aggregation in microwells and subsequently transferred to rotary orbital culture. (B) MP incorporation per aggregate at various MP to cell seeding ratios. (C) Alexa Fluor 594 labeled-MPs (red) were readily incorporated and persisted within the ESC aggregates for up to 14 days of culture.

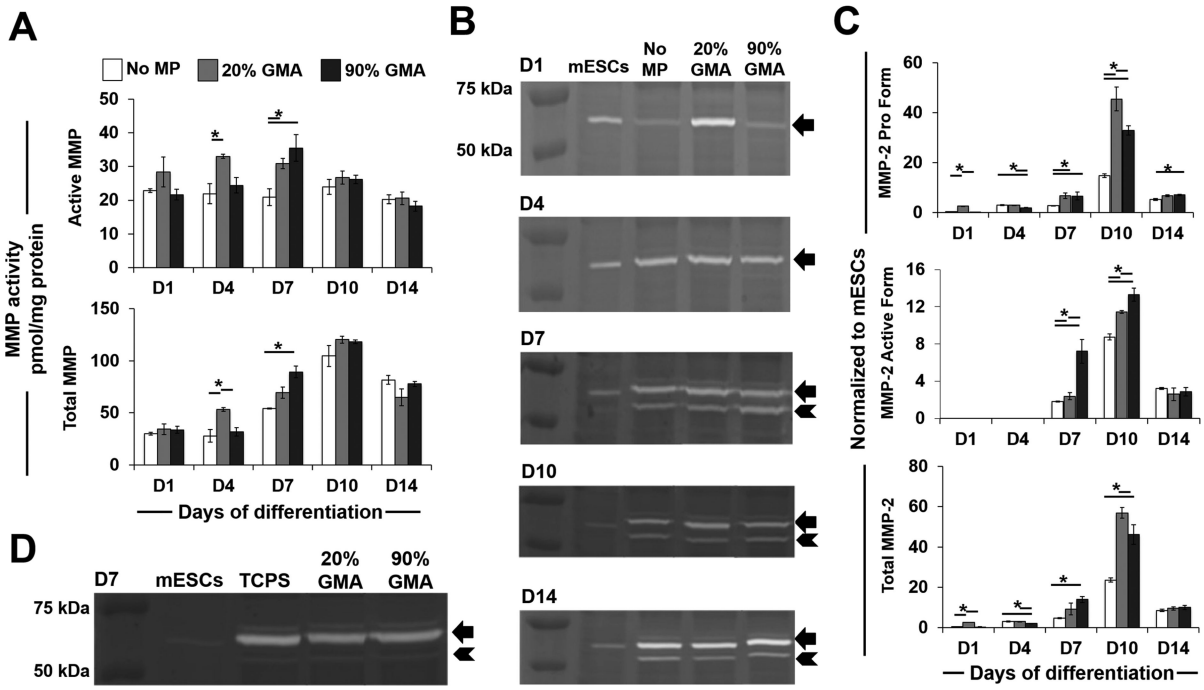

Figure 2.

GMA MP incorporation increases MMP levels in ESC aggregates. (A) Overall MMP levels, including active and total MMP activities for spheroids with and without MPs, were analyzed using a FRET-conjugated cleavable peptide-based assay. (B-C) Expression levels of pro (arrow) and active (arrowhead) forms of MMP-2 in spheroid lysates were analyzed by gel zymography (B) and densitometry (C) analysis. (D) Zymography for MMP-2 in D7 spheroids plated on either TCPS or GMA-coated TCPS. Arrow indicates MMP-2 pro form, and arrowhead indicates MMP-2 active form. * $P<0.05$ ($n \geq 3$)

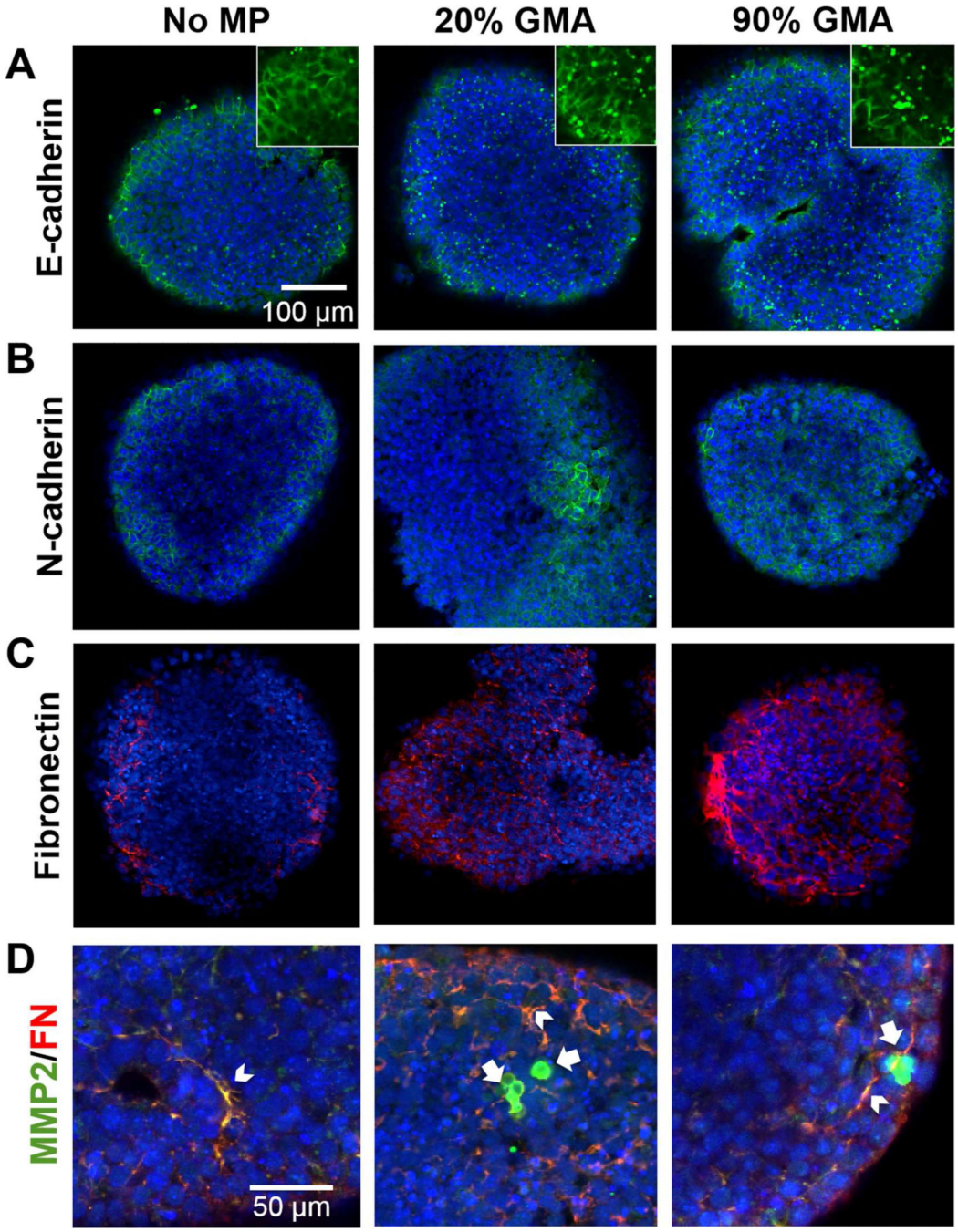

Figure 3.

MP incorporation modulates expression patterns of cadherins, fibronectin, and MMP-2 in day 10 ESC aggregates. Expression levels of E-cadherin (A, green), N-cadherin (B, green), fibronectin (C, red), and MMP-2 (D, green) were analyzed by immunostaining. Arrowhead indicates the co-localization of MMP-2 and fibronectin (yellow), and arrow indicates a region of concentrated MMP2 expression (green).

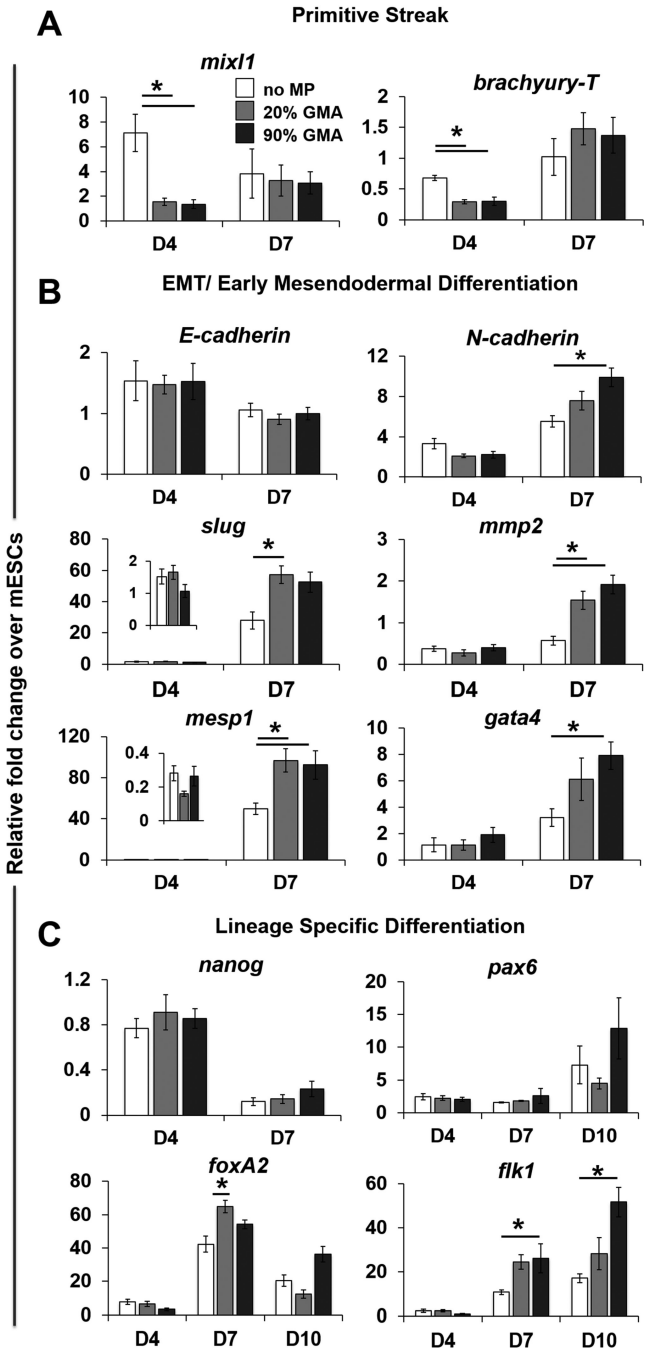

Figure 4.

MP incorporation modulates gene expression patterns. The gene expression of (A) primitive streak markers (*mixl1* and *brachyury-T*), (B) EMT and early mesendodermal markers (*E-cadherin N-cadherin, Slug, mmp2, mesp1*, and *gata4*), and (C) lineage-specific markers (*nanog, pax6, foxA2*, and *flk1*) in aggregates at days 4, 7, or 10 of differentiation was analyzed using real-time PCR and normalized to housekeeping gene *s18*. Relative fold changes over ESC gene expression levels were calculated for all samples. * $P<0.05$ ($n \geq 4$).

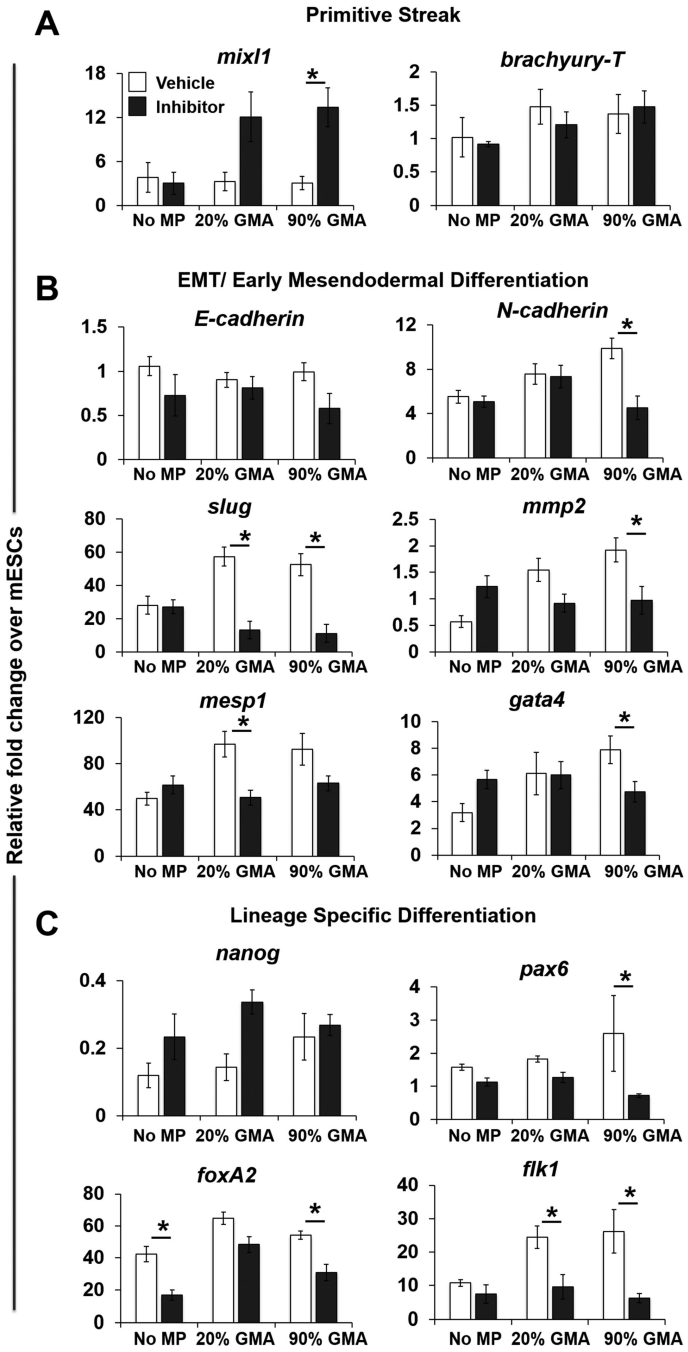

Figure 5.

Inhibition of MMP abrogates MP-induced changes in EMT-related and lineage-specific gene expression in day 7 ESC aggregates. The aggregates were treated with an MMP inhibitor (50 μM Ro32-3555) from day 5 of differentiation. Gene expression levels of primitive streak markers (A), EMT and early mesendodermal markers (B), and lineage specific markers (C) at day 7 of differentiation were determined by real-time PCR. Relative fold change over ESC gene expression level was calculated for all samples. * $P<0.05$ ($n \geq 4$).

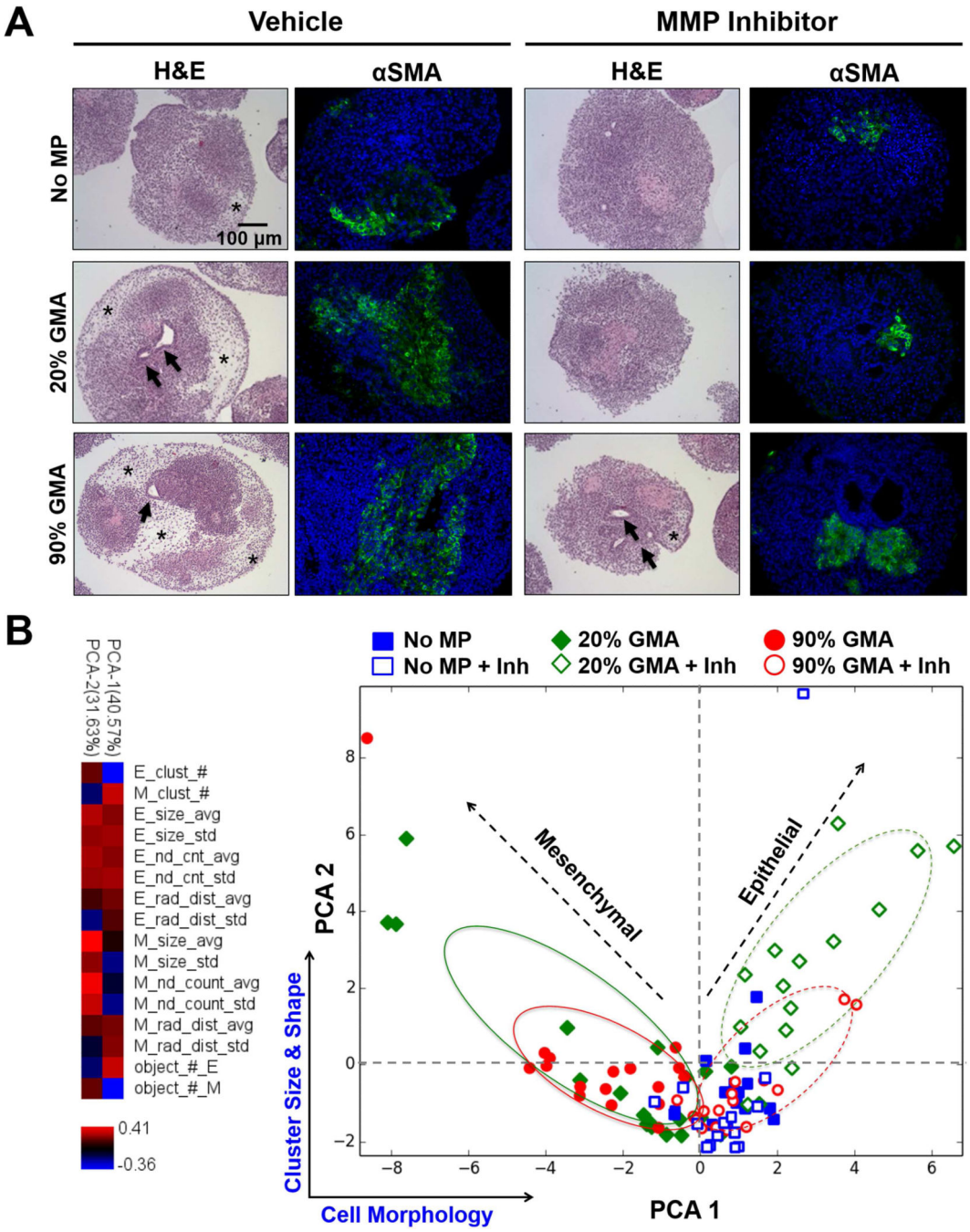

Figure 6.

MP incorporation enhances MMP-dependent mesenchymal morphogenesis in day 14 aggregates. (A) H&E staining and α-smooth muscle actin (α-SMA) immunostaining of D14 ESC aggregates with vehicle (ethanol) or MMP inhibitor (Ro32-3555) treatment. Star indicates mesenchymal regions, and arrows indicate cavitated structures. α-SMA was labeled as green and nuclei (blue) were stained with Hoechst dye. (B) The variance in mesenchymal phenotype between different experimental groups was captured by a PCA model based on cell morphology and cell cluster size and shape.

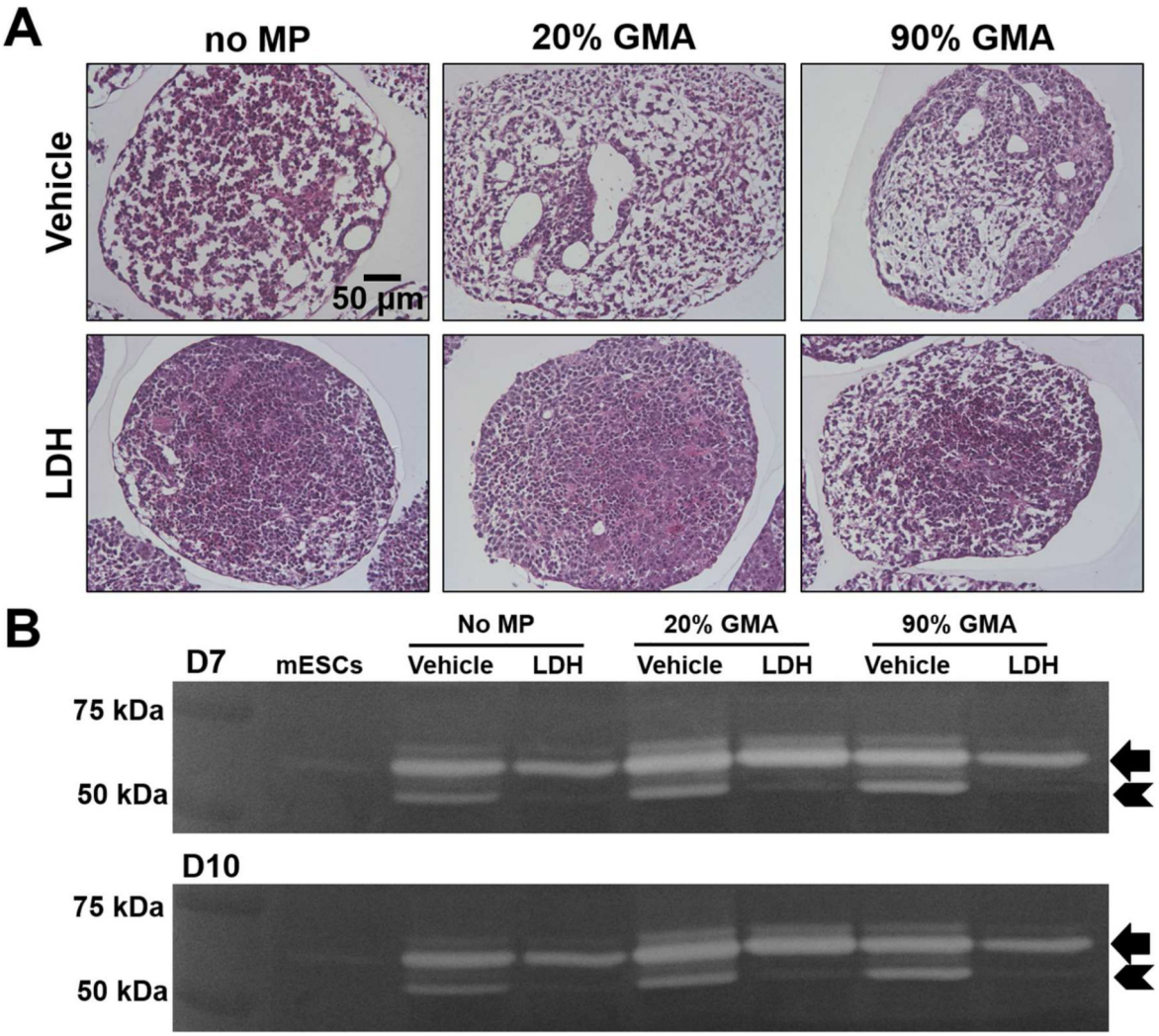

Figure 7.

pSMAD 1/5/8 inhibition reduces MP induced-mesenchymal morphology and MMP-2 activation. ESC aggregates were treated with pSMAD 1/5/8 inhibitor (LDH-193189) from day 3– day 14 of differentiation. (A) Morphology changes were evaluated by H&E staining on day 14 and (B) the expression levels of pro and active forms of MMP-2 were analyzed by zymography on days 7 and 10 of differentiation.